Proc. Natl. Acad. Sci. USA
Vol. 93, pp. 8836–8840, August 1996
Biochemistry

Zinc- and iron-rubredoxins from *Clostridium pasteurianum* at atomic resolution: A high-precision model of a ZnS_4 coordination unit in a protein

(x-ray crystallography/zinc fingers/iron-sulfur/metal homeostasis)

ZBIGNIEW DAUTER*, KEITH S. WILSON*, LARRY C. SIEKER†, JEAN-MARC MOULIS‡, AND JACQUES MEYER‡§

*European Molecular Biology Laboratory, Outstation Hamburg, c/o Deutsches Elektronen Synchrotron, Notkestrasse 85, 22603 Hamburg, Germany; †Department of Biological Structure, SM-20, University of Washington, Seattle, WA 98195; and ‡Laboratoire Métalloprotéines, Département de Biologie Moléculaire et Structurale, Commissariat à l'Energie Atomique–Grenoble, 17 avenue des Martyrs, 38054 Grenoble, France

Communicated by David Eisenberg, University of California, Los Angeles, CA, May 15, 1996 (received for review December 27, 1995)

ABSTRACT **The $Zn(S_{cys})_4$ unit is present in numerous proteins, where it assumes structural, regulatory, or catalytic roles. The same coordination is found naturally around iron in rubredoxins, several structures of which have been refined at resolutions of, or near to, 1 Å. The fold of the small protein rubredoxin around its metal ion is an excellent model for many zinc finger proteins. Zn-substituted rubredoxin and its Fe-containing counterpart were both obtained as the products of the expression in *Escherichia coli* of the rubredoxin-encoding gene from *Clostridium pasteurianum*. The structures of both proteins have been refined with an anisotropic model at atomic resolution (1.1 Å, $R = 8.3\%$ for Fe-rubredoxin, and 1.2 Å, $R = 9.6\%$ for Zn-rubredoxin) and are very similar. The most significant differences are increased lengths of the M–S bonds in Zn-rubredoxin (average length, 2.345 Å) as compared with Fe-rubredoxin (average length, 2.262 Å). An increase of the CA-CB-SG-M dihedral angles involving Cys-6 and Cys-39, the first cysteines of each of the Cys-Xaa-Xaa-Cys metal binding motifs, has been observed. Another consequence of the replacement of iron by zinc is that the region around residues 36–46 undergoes larger displacements than the remainder of the polypeptide chain. Despite these changes, the main features of the FeS_4 site, namely a local 2-fold symmetry and the characteristic network of N–H. . .S hydrogen bonds, are conserved in the ZnS_4 site. The Zn-substituted rubredoxin provides the first precise structure of a $Zn(S_{cys})_4$ unit in a protein. The nearly identical fold of rubredoxin around iron or zinc suggests that at least in some of the sites where the metal has mainly a structural role—e.g., zinc fingers—the choice of the relevant metal may be directed by its cellular availability and mobilization processes rather than by its chemical nature.**

There is a large number of zinc-containing proteins in which the metal assumes either catalytic or stabilizing roles (1). Among the diverse coordinations of zinc found in these proteins, the sites in which the metal has four cysteine ligands have recently attracted increased attention. $Zn(S_{cys})_4$ sites have long been known in alcohol dehydrogenases and in aspartate transcarbamylase. A structural role is proposed in the former, whereas in the latter, the zinc site is thought to mediate the allosteric transition (1). In recent years, zinc has also been found in a wide range of proteins involved in regulation of gene expression (2–6), electron transfer (7), or DNA repair (8). In the latter, zinc and one of its cysteine ligands are involved in the catalytic mechanism (8). Although several crystal structures of proteins containing $Zn(S_{cys})_4$ sites are available (2, 7, 9–11), the resolution, at best 1.8 Å, is insufficient to provide a very accurate geometry of the ZnS_4 unit. Such information can be obtained either from higher resolution structures of the above mentioned proteins or from structurally well characterized model proteins in which a ZnS_4 site has been engineered.

Rubredoxins (Rds) are attractive proteins for the latter approach. The active site of these small (≈6 kDa) nonheme iron proteins is arranged around an iron atom tetrahedrally coordinated to four cysteinyl sulfurs. Rds have been structurally characterized in considerable detail, including five high resolution (1.0–1.8 Å) crystal structures (12–18). The iron binding motif of Rd provides an excellent structural model for the metal environment of many members of the zinc finger family (19). An interesting property of Rd is the possibility of replacing the iron atom with other metals, including cobalt (20), nickel (21), and, of particular relevance here, zinc (22). The metal-substituted Rd referred to above have all been prepared by removal of the iron atom from the native protein and subsequent incorporation of the heterometal into the apoprotein. Recently, the *Clostridium pasteurianum* Rd gene has been expressed in *Escherichia coli* (23–26), where Zn-substituted Rd (ZnRd) is produced along with the iron-containing protein (FeRd; refs. 24 and 27). This provided a convenient and abundant source of ZnRd and a very good opportunity to obtain a precise structure of the ZnS_4 unit in a protein. Accordingly, here we report and compare the atomic resolution crystal structures of both Zn- and Fe-recombinant *C. pasteurianum* Rds produced in *E. coli*.

MATERIALS AND METHODS

Overexpression of the *C. pasteurianum* (ATCC 6013) Rd gene (23) and purification of the recombinant FeRd and ZnRd (27) have been described.

Crystallization. Crystals of recombinant FeRd were obtained as described for the protein purified from *C. pasteurianum* (28). The same conditions were used for ZnRd, but in this instance, sitting drop vapor equilibration was used in conjunction with seeding to prevent overnucleation. The drop contained 30 μl of 0.8–1.6 mM protein solution in 0.82 M (20% saturated) ammonium sulfate/30 mM citrate, pH 4.0. This was equilibrated against a reservoir solution containing 2.46 M (60% saturated) ammonium sulfate and 100 mM citrate (pH 4.0). After equilibration for a day at 23°C, two to three small seed crystals, washed in buffered 2 M ammonium sulfate, were introduced into the drop. After a few days, these crystals developed into large colorless squat

The publication costs of this article were defrayed in part by page charge payment. This article must therefore be hereby marked "*advertisement*" in accordance with 18 U.S.C. §1734 solely to indicate this fact.

Abbreviation: Rd, rubredoxin.

Data deposition: The atomic coordinates have been deposited with the Protein Data Bank, Chemistry Department, Brookhaven National Laboratory, Upton, NY 11975 [references 1IRO (FeRd) and 1IRN (ZnRd)].

§To whom reprint requests should be addressed.

trigonal prisms. The crystallization was completed by allowing the drops to equilibrate against buffered 2.8 M ammonium sulfate solution. To collect high-resolution diffraction data, a crystal of approximate dimensions 0.5 × 0.5 × 0.2 mm was mounted in a capillary.

X-Ray Data Collection. Diffraction data on both crystals, ZnRd and FeRd, were collected using a very similar protocol with synchrotron radiation from the European Molecular Biology Laboratory X11 beam line at the DORIS ring, Deutsches Elektronen Synchrotron (Hamburg, Germany). A 180-mm diameter MAR Research (Hamburg, Germany) imaging plate scanner was used as detector. A summary of data collection and processing is given in Table 1. For both crystals, data were collected at room temperature, and the intensities were integrated, scaled, and merged using the program DENZO (29). Data from both crystals extended to atomic resolution, 1.2 Å for ZnRd and 1.1 Å for FeRd, with high completeness and average ratio $I/\sigma(I)$ above three in the highest resolution shell (Table 1). Cell dimensions were postrefined on the basis of intensities of partial reflections as follows: for ZnRd, $a = 64.10$ Å and $c = 33.05$ Å; and for FeRd, $a = 64.04$ Å and $c = 32.51$ Å, both in space group R3. Wilson plots (30) gave estimates for the overall B factors of 10.2 Å^2 and 10.6 Å^2, respectively.

Refinement. For both structures the refinement protocol was the same, but the refinements for FeRd and ZnRd were carried out completely independently and are summarized in Table 2. The starting model was the 5RXN (*C. pasteurianum* Rd) entry in the Protein Data Bank (31) without the water atoms. Throughout refinement the Engh and Huber (32) stereochemical restraints were applied to the protein. Metal-site geometries were not restrained.

The models were first refined using the program PROLSQ (33) with ARP (34) to locate solvent water molecules in an objective and automatic way. Next, SHELXL-93 (35) was used with isotropic and subsequently anisotropic atomic temperature factors and conjugate gradient option. Finally, several cycles of SHELXL-93 refinement with full-matrix least-squares option was performed with blocks of atoms, each containing ≈20 amino acids, overlapping by one residue. All water molecules were refined with unit occupancy. Several residues with alternate side chain conformations were identified by inspecting the $3F_o$-$2F_c$ and F_o-F_c electron density maps using FRODO (36); occupancies of individual conformers were constrained to sum to unity.

The SHELXL refinement was performed against F^2 with Friedel related reflections treated as independent. Structure factor amplitudes (Fs) (after averaging the Friedel related pairs) were used only to calculate $3F_o$-$2F_c$ and F_o-F_c Fourier syntheses and to compute the conventional R factor. No σ cutoff was applied in any refinement step. R_{free} validation (37) was used, based on a subset of 5% of reflections. R_{free} was not sufficient to assess the significance of small extensions of the final model, such as multiple conformations of several side chains; here local criteria in terms of details of the density maps were more relevant. All reflections were included in the final cycles. A detailed description of the structure analysis will be published elsewhere.

Table 1. Summary of data collection

	ZnRd	FeRd
Space group	R3	R3
Resolution limits, Å	25–1.2	20–1.1
Unique reflections	15,659	20,052
Completeness, %	99	94
$R(I)_{merge}$ overall, %	5.9	4.7
$R(I)_{merge}$ at highest resolution, %	26.0	26.2
$I/\sigma(I)$ overall	19	24
$I/\sigma(I)$ at highest resolution	3.6	3.2

Table 2. Refinement statistics

	ZnRd	FeRd
No. of residues	53	53
Side chains in double conformations	3*	6†
No. of protein atom sites	423	433
No. of solvent water sites	87	110
Total number of reflections used	28,046	34,415
No. of reflections after merging Friedels	15,815	19,620
R1 for all reflections‡	0.1068	0.0903

*Residues Thr-5, Pro-15, and Glu-50.
†Residues Thr-5, Ile-12, Pro-15, Lys-31, Leu-41, and Glu-50.
‡$R1 = \Sigma \, ||F_0| - |F_c|| / \Sigma \, |F_0|$.

RESULTS AND DISCUSSION

Accuracy of the Structures. Since the final models were refined by block-matrix least-squares, all atomic positional and thermal parameters are accompanied by their standard deviations estimated from the inversion of the matrix. Therefore it is possible to discuss the positional accuracy of individual atoms or fragments of the model, in contrast to the situation in most macromolecular structure analyses, where only overall or mean accuracy can be estimated indirectly—e.g., from the σ_A plot (38). The main chain bond length errors are below 0.02 Å, except for the first two and last two observed residues (0.07 Å). Since these residues belong to the most flexible regions of the structure, they have the highest temperature factors and the weakest electron density. The last expected residue of the sequence (Glu-54) could not be modeled in either of the two structures. In addition, the atoms at the end of the poorly defined Lys-2 side chain (CD, CE, and NZ in ZnRd; CE and NZ in FeRd) have been assigned an occupancy of zero, as there was no significant electron density. However, all of these poorly defined atoms are far from the metal site, and any small error in their positioning in the model is unlikely to have any bearing on the interpretation of the MS_4 site.

As expected, estimated atomic coordinate errors correlate strongly with the corresponding temperature factors. The mean coordinate errors and temperature factors are plotted as a function of residue number for FeRd and ZnRd in Fig. 1.

Structure of FeRd. The structural model of FeRd obtained here with a resolution of 1.1 Å was superimposed on the previous one refined at 1.2 Å (ref. 12; Protein Data Bank entry 5RXN), by least-squares fitting using the 53 observed CA atoms. The overall rms distance between the corresponding CA atoms of the two structures was 0.09 Å, and the distance between the two Fe atoms was 0.032 Å (Fig. 2, filled circles). Therefore, the two models are very similar and the presently refined structure of FeRd will not be discussed in further detail here, but only referred to in the next section for comparison with ZnRd.

Structure of ZnRd and of the ZnS_4 Site. The structural model of ZnRd at 1.2-Å resolution has been superimposed on the 1.1 Å resolution model of FeRd using a least-squares rigid body fit on the CA atoms (Fig. 3). The overall rms distance between the corresponding CA atoms of the two structures was 0.12 Å, a value ≈1.3 times larger than the one determined for the two high-resolution structures available for FeRd obtained by independent groups (Fig. 2). The distance between the Fe and the Zn atoms is 0.146 Å—i.e., almost 4 times the distance between the Fe atom positions in the 1.2-Å and 1.1-Å resolution models of FeRd. In contrast to the superposition of the two differently refined FeRd structures, the discrepancies between the positions of the CA atoms of the two structures are not distributed randomly (Fig. 2); larger differences (range 0.1–0.36 Å) are observed for residues 36–46 than elsewhere in the structure, the most shifted atoms belonging to residues 44–46 (rms >0.21 Å). This part of the protein is a loop including two of the iron ligands (Cys-39 and Cys-42) and is clearly the only part of the Rd

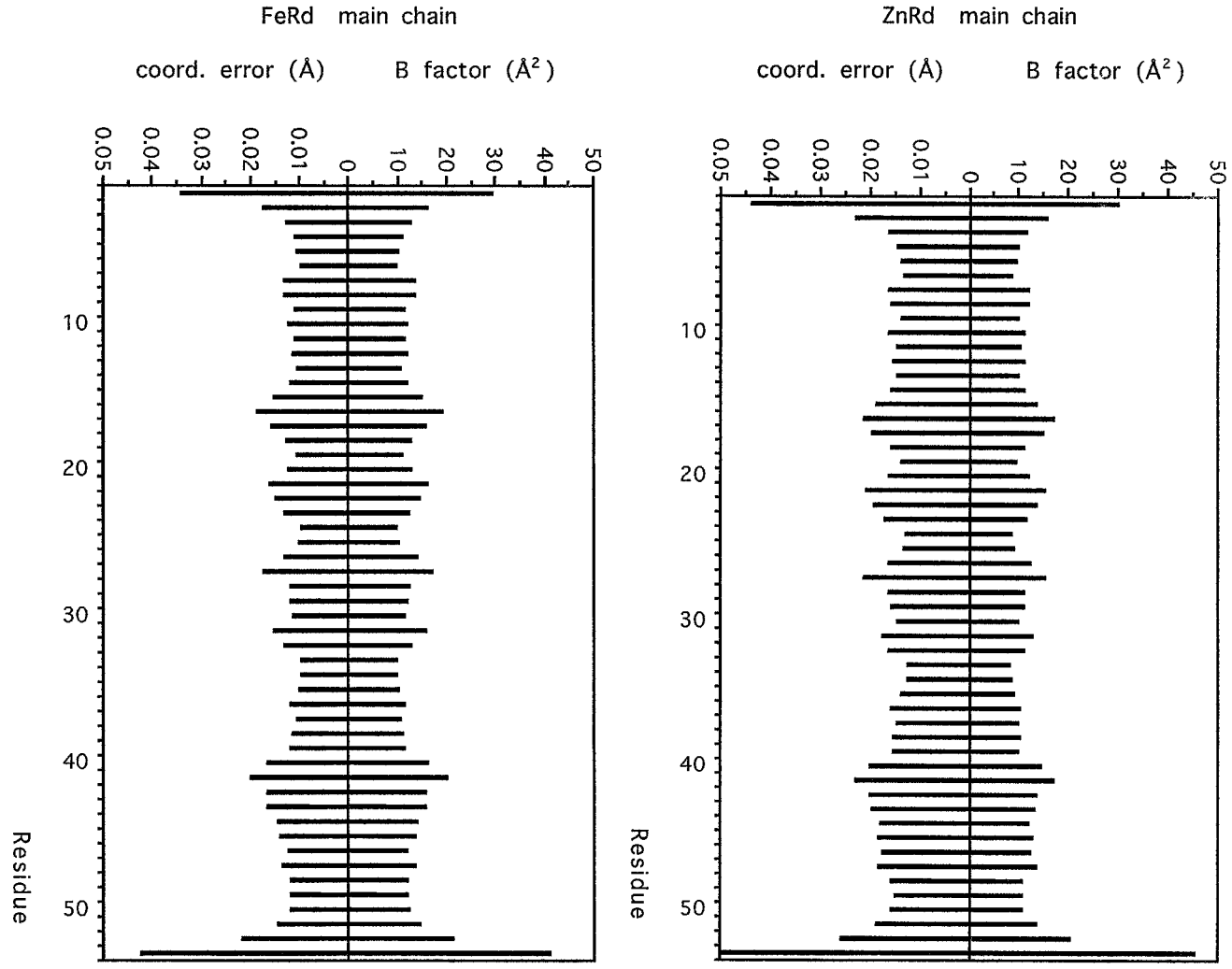

FIG. 1. Coordinate errors averaged over main chain atoms of each residue and averaged temperature factors as a function of residue number for (*Left*) FeRd and (*Right*) ZnRd. The plots clearly illustrate that the coordinate errors are correlated with *B* factors.

structure that significantly senses the replacement of Fe by Zn.

The distances and angles of the ZnS_4 site are compared with the corresponding parameters of the FeS_4 site in Table 3 and Fig. 4. The main difference between the FeS_4 and ZnS_4 structural units is an increase of ≈0.08 Å in the metal–sulfur bond lengths. This was expected from the known structures of synthetic analogues (refs. 39–41; see below). Two longer (≈2.365 Å) and two shorter (≈2.32 Å) Zn–S bonds are observed in ZnRd (Table 3), in keeping with the local 2-fold symmetry of the FeS_4 site in all Rds (18). This shows that the polypeptide structural framework imposes similar constraints on both MS_4 (M = Fe^{3+} or Zn^{2+}) units, as witnessed by the similar networks of hydrogen bonds (see below). Similarly, the S–M–S angles show only marginal differences between the two proteins, with a set of four at ≈112.0° and a set of two at ≈104.0°. Thus, very similar distortions from ideal tetrahedral coordination by compression along an approximate 2-fold axis passing through the metal ion occur in both the FeS_4 and the ZnS_4 sites. Since the crystal packing shows no intermolecular interactions in the region of the metal site, the similarity of the geometries of these sites are unlikely to result from such interactions. The CA-CB-SG-M dihedral angles undergo small variations upon replacement of iron by zinc. Those involving Cys-6 and Cys-39 are more affected than the other two. The distribution of N–H. . .S hydrogen bonds is the same in both proteins, in agreement with the similarities outlined above. Nevertheless, the N–H. . .S distances are not uniformly modified by the Fe/Zn substitution. The structural changes imposed by the metal substitution are not isotropically distributed, in keeping with the superposition of the FeRd and ZnRd structures, which shows that the region around residues 36–46 undergoes larger structural changes than the rest of the protein.

Comparison with ZnS_4 Units in Synthetic Compounds. Few chemical models of zinc tetrahedrally coordinated to thiolates have been synthesized and structurally characterized. They all involve aromatic thiolate ligands, whereas cysteinates only occur in biological ZnS_4 structures. Nevertheless, the Zn–S distances measured for ZnRd (Table 3) are within the range of those observed in $Zn(SC_6H_5)_4^{2-}$ (2.329–2.363 Å; ref. 40) and in $Zn(S\text{-}2,3,5,6\text{-}Me_4C_6H)_4^{2-}$ (2.36 Å; ref. 41). Somewhat surprisingly, the values of the S–Zn–S angles in $Zn(SC_6H_5)_4^{2-}$ (two in the 96–100° range and four in the 112–121° range; ref. 40) have a greater distortion along the 2-fold axis than the one found in the protein. Similar distortions were observed for several divalent metal ion complexes and were assigned to crystal packing forces (40). The synthetic analogues also displayed some heterogeneity in Zn–S bond length, but the trend was one shorter (2.329 Å) bond and three longer (2.357 Å, 2.362 Å, and 2.363 Å) ones, typical of trigonal pyramidal coordination (40), rather than two and two, as in Rd.

Comparison of the Differences Between ZnRd and FeRd with Those Between Oxidized and Reduced FeRd. The structural differences between the active sites of FeRd and ZnRd (Table 3 and Fig. 4) are associated with the replacement of a

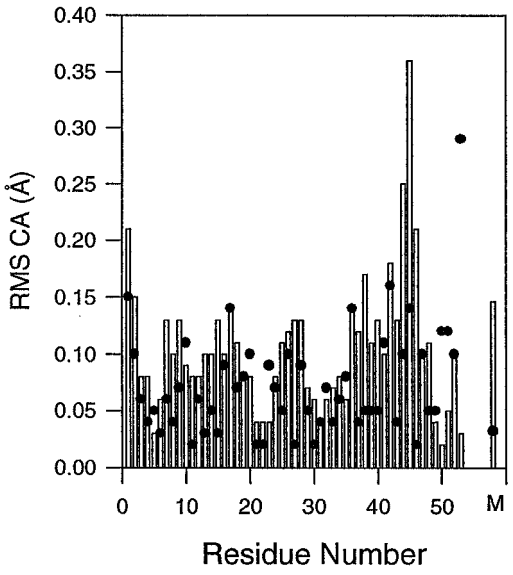

FIG. 2. Differences between CA positions of FeRd and ZnRd (bars) and between the present FeRd model and that from 5RXN (filled circles). Both pairs of structures were overlapped by least-squares on 53 CA atoms. M stands for the metal atom.

trivalent metal (a ferric ion) by a divalent one (a zinc ion). Although the refinement of oxidized (ferric ion) and reduced (ferrous ion) Rd from *Pyrococcus furiosus* at 1.8 Å (17) required restraints that impose limits on the significance of the atom adjustments, it is relevant to compare these differences with the ones reported here between FeRd and ZnRd. The replacement of iron by zinc induces a lengthening (average, 0.08 Å) of the M–S bonds significantly larger than that resulting from the reduction of the ferric ion (0.035 Å). In contrast, the CA-CB-SG-M dihedral angles undergo larger changes (−3 to +10°) upon reduction of FeRd (17) than upon replacement of iron by zinc (+0.2 to +3.8°, Table 3). As for the average shortening of the N–H. . . S hydrogen bond lengths involving cysteinate sulfur atoms, the values are similar: 0.085 Å (17) and 0.083 Å (Table 3). One possibility is that the shortenings arise mainly from electronic effects on the MS4 site. These similar values would then suggest that the extra electron gained upon reduction of Fe(III) Rd is distributed over the four cysteinyl sulfur atoms, as theoretically predicted (42).

CONCLUSIONS

An increasing number of proteins, including zinc fingers, are known to contain the ZnS_4 unit (2, 3, 5–7), but in those cases where crystal structures are available, the resolution is insufficient to provide an accurate geometry. The present structure of ZnRd is the first precise description of a zinc ion tetrahedrally coordinated to four cysteine residues of a protein and it affords accurate Zn–S bond lengths that will be useful as target distances for the determination of the structure of other ZnS_4 proteins (19). Since ZnRd and FeRd are almost isostructural, this work also shows that the canonical folding of the Cys-Xaa-Xaa-Cys binding motifs does not rely on the presence of a specific metal atom. It may be inferred that the DNA binding properties exhibited by a number of Zn-containing proteins are not dependent on the exact chemical identity of the metal but rather on its ability to induce the metal-aided folding of these proteins. This brings forth the question of why zinc is a ubiquitous component of zinc finger proteins, whereas *E. coli* is apparently unable to differentiate between iron and zinc for incorporation into heterologous Rd. The metal selectivity may be ensured by host cell-dependent mechanisms of metal homeostatis and incorporation into appro-

Table 3. Comparison of metal coordination in ZnRd and in FeRd

	ZnRd	FeRd	Diff., Zn − Fe
Distances, Å			
M-SG6	2.365	2.287	+0.078
M-SG9	2.331	2.249	+0.082
M-SG39	2.368	2.283	+0.085
M-SG42	2.313	2.230	+0.084
Mean			+0.082
Estimated from SHELXL	0.004	0.003	
Angles, °			
S6-M-SG9	113.0	113.4	−0.4
S6-M-S39	111.9	110.1	+1.8
S6-M-S42	104.5	104.3	+0.2
S9-M-S39	104.1	104.6	−0.5
S9-M-S42	111.8	112.7	−0.9
S39-M-S42	111.7	111.9	−0.2
Estimated from SHELXL	0.1	0.1	
Dihedral angles, °			
CA-CB-SG6-M	173.5	169.7	+3.8
CA-CB-SG9-M	94.0	93.8	+0.2
CA-CB-SG39-M	179.0	175.8	+3.2
CA-CB-SG42-M	88.7	88.1	+0.6
Hydrogen bond distances, Å			
SG6. . .N8	3.571	3.677	−0.106
SG6. . .N9	3.501	3.646	−0.145
SG9. . .N11	3.454	3.488	−0.034
SG39. . .N41	3.432	3.541	−0.109
SG39. . .N42	3.553	3.578	−0.025
SG42. . .N44	3.764	3.844	−0.080
Mean			−0.083

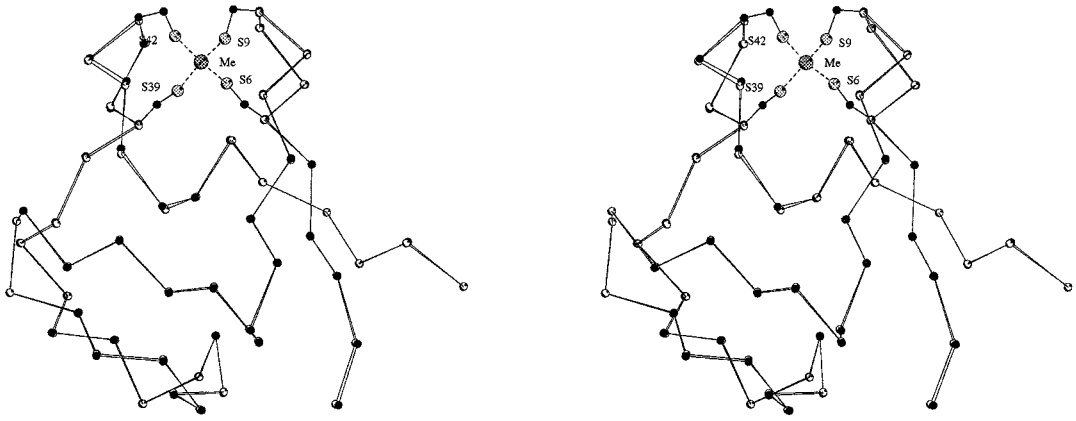

FIG. 3. Stereo CA trace of FeRd (filled circles) and ZnRd (open circles). The overlap was based on 53 CA atoms. In this view the local 2-fold axis through the metal atom is vertical.

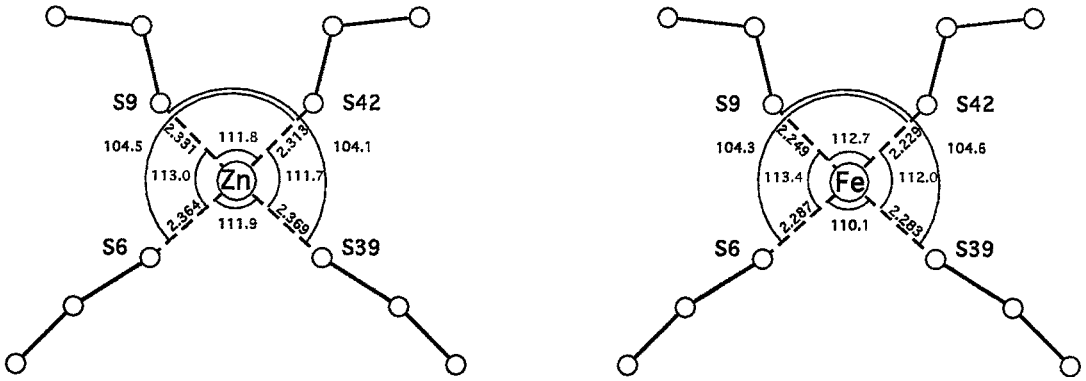

FIG. 4. Geometry of metal sites of FeRd (*Right*) and ZnRd (*Left*).

priate proteins. Indeed, an overwhelming majority of zinc finger proteins have been described in Eucarya, in which proteins, often distinct from those found in Bacteria, are involved in metal mobilization. For instance, metallothionein seems to participate in the regulation of the bioavailability of zinc and in the activity of at least some DNA-binding zinc proteins (43). It may be anticipated that such a fine modulation of metal binding to potential ligands is different in organisms similar to *E. coli*, in which various sets of proteins are involved in the mobilization of metals.

In addition to being a highly accurate structural model, ZnRd may be anticipated to afford functional models for the reactivity of some ZnS_4 sites in enzymes. Indeed, although such sites usually appear to have a structural role, an interesting case of reactivity has been discovered in the *E. coli* Ada DNA repair enzyme: the methyl group of DNA methylphosphotriester is attacked by, and transferred onto, one of the cysteinate ligands of the Zn ion (8). ZnRd is a promising tool for the investigation of such reactivities. In addition to the high resolution structure reported here, the metal site of this protein has recently been proven to be amenable to molecular engineering (44).

We acknowledge the support of the European Community through Contract BIO2CT-920524 (to K.S.W.) for part of this work.

1. Vallee, B. L. & Auld, D. S. (1993) *Acc. Chem. Res.* **26,** 543–551.
2. Luisi, B. F., Xu, W. X., Otwinowski, Z., Freedman, L. P., Yamamoto, K. R. & Sigler, P. B. (1991) *Nature (London)* **352,** 497–505.
3. Omichinski, J. G., Clore, G. M., Schaad, O., Felsenfeld, G., Trainor, C., Appella, E., Stahl, S. J. & Gronenborn, A. M. (1993) *Science* **261,** 438–446.
4. O'Halloran, T. V. (1993) *Science* **261,** 715–725.
5. Perez-Alvarado, G. C., Miles, C., Michelsen, J. W., Louis, H. A., Winge, D. R., Beckerle, M. C. & Summers, M. F. (1994) *Nat. Struct. Biol.* **1,** 388–398.
6. Landro, J. A., Schmidt, E., Schimmel, P., Tierney, D. L. & Penner-Hahn, J. E. (1994) *Biochemistry* **33,** 14213–14220.
7. Tsukihara, T., Aoyama, H., Yamashita, E., Tomizaki, T., Yamaguchi, H., Shinzawa-Itoh, K., Nakashima, R., Yaono, R. & Yoshikawa, S. (1995) *Science* **269,** 1069–1074.
8. Myers, L. C., Terranova, M. P., Ferentz, A. E., Wagner, G. & Verdine, G. L. (1993) *Science* **261,** 1164–1167.
9. Eklund, H., Nordström, B., Zeppezauer, E., Söderlund, G., Ohlsson, I., Boiwe, T., Söderberg, B.-O., Tapia, O., Brändén, C.-I. & Åkeson, Å (1976) *J. Mol. Biol.* **102,** 27–59.
10. Monaco, H. L., Crawford, J. L. & Lipscomb, W. N. (1978) *Proc. Natl. Acad. Sci. USA* **75,** 5276–5280.
11. Al-Karadaghi, S., Cedergren-Zeppezauer, E. S., Hövmoller, S., Petratos, K., Terry, H. & Wilson, K. S. (1994) *Acta Crystallogr. D* **50,** 793–807.
12. Watenpaugh, K. D., Sieker, L. C. & Jensen, L. H. (1980) *J. Mol. Biol.* **138,** 615–633.
13. Frey, M., Sieker, L., Payan, F., Haser, R., Bruschi, M., Pepe, G. & LeGall, J. (1990) *J. Mol. Biol.* **197,** 525–541.
14. Stenkamp, R. E., Sieker, L. C. & Jensen, L. H. (1990) *Proteins Struct. Funct. Genet.* **8,** 352–364.
15. Adman, E. T., Sieker, L. C. & Jensen, L. H. (1991) *J. Mol. Biol.* **217,** 337–352.
16. Dauter, Z., Sieker, L. C. & Wilson, K. S. (1992) *Acta Crystallogr. B* **48,** 42–59.
17. Day, M. W., Hsu, B. T., Joshua-Tor, L., Park, J.-B., Zhou, Z. H., Adams, M. W. W. & Rees, D. C. (1992) *Protein Sci.* **1,** 1494–1507.
18. Sieker, L. C., Stenkamp, R. E. & LeGall, J. (1994) *Methods Enzymol.* **243,** 203–216.
19. Schwabe, J. W. R. & Klug, A. (1994) *Nat. Struct. Biol.* **1,** 345–349.
20. May, S. W. & Kuo, J.-Y. (1978) *Biochemistry* **17,** 3333–3338.
21. Kowal, A. T., Zambrano, I. C., Moura, I., Moura, J. J. G., LeGall, J. & Johnson, M. K. (1988) *Inorg. Chem.* **27,** 1162–1166.
22. Blake, P. R., Park, J.-B., Zhou, Z. H., Hare, D. R., Adams, M. W. W. & Summers M. F. (1992) *Protein Sci.* **1,** 1508–1521.
23. Mathieu, I., Meyer, J. & Moulis, J.-M. (1992) *Biochem. J.* **285,** 255–262.
24. Eidsness, M. K., O'Dell, S. E., Kurtz, D. M., Jr., Robson, R. L. & Scott, R. A. (1992) *Protein Eng.* **5,** 367–371.
25. Mathieu, I. & Meyer, J. (1993) *FEMS Microbiol. Lett.* **112,** 223–228.
26. Moulis, J.-M., Davasse, V. & De Jésus, F. (1994) *BioMetals* **7,** 272–278.
27. Pétillot, V., Forest, E., Mathieu, I., Meyer, J. & Moulis, J.-M. (1993) *Biochem. J.* **296,** 657–661.
28. Herriott, J. R., Sieker, L. C., Jensen, L. H. & Lovenberg, W. (1970) *J. Mol. Biol.* **50,** 391–406.
29. Otwinowski, Z. & Minor, W. (1993) DENZO: A Film Processing Program for Macromolecular Crystallography. (Yale Univ. Press, New Haven, CT).
30. Wilson, A. J. C. (1942) *Nature (London)* **150,** 151–152.
31. Bernstein, F. C., Koetzle, T. F., Williams, G. J. B., Mayer, E. F., Brice, M. D., Rodgers, J. R., Kennard, O., Simanouchi, T. & Tasumi, M. (1977) *J. Mol. Biol.* **112,** 535–542.
32. Engh, R. A. & Huber, R. (1991) *Acta Crystallogr. A.* **47,** 392–400.
33. Konnert, J. H. & Hendrickson, W. A. (1980) *Acta Crystallogr. A* **36,** 344–350.
34. Lamzin, V. S. & Wilson, K. S. (1993) *Acta Crystallogr. D* **49,** 129–147.
35. Sheldrick, G. M. & Schneider, T. R (1996) *Methods Enzymol.*, in press.
36. Jones, T. A. (1985) *Methods Enzymol.* **115,** 157–171.
37. Brünger, A. (1993) *Acta Crystallogr. D* **49,** 24–36.
38. Read, R. J. (1986) *Acta Crystallogr. A* **42,** 140–149.
39. Lane, R. W., Ibers, J. A., Frankel, R. B., Papaefthymiou, G. C. & Holm, R. H. (1977) *J. Am. Chem. Soc.* **99,** 84–98.
40. Swenson, D., Baenziger, N. C. & Coucouvannis, D. (1978) *J. Am. Chem. Soc.* **100,** 1932–1934.
41. Gruff, E. S. & Koch, S. A. (1989) *J. Am. Chem. Soc.* **111,** 8762–8763.
42. Noodleman, L., Norman, J. G., Jr., Osborne, J. H., Aizman, A. & Case, D. A. (1985) *J. Am. Chem. Soc.* **107,** 3418–3426.
43. Zeng, J., Vallee, B. L. & Kägi, J. H. R. (1991) *Proc. Natl. Acad. Sci. USA* **88,** 9984–9988.
44. Meyer, J., Gaillard, J. & Lutz, M. (1995) *Biochem. Biophys. Res. Commun.* **212,** 827–833.